The Dynamic Characteristics of Curved Wall Fluidic Thrusters

The Dynamic Characteristics of Curved Wall Fluidic Thrusters

Osamu KINOSHITA *, Masao MURAKAMI ** and Yasujiro OSHIMA ***

(Received November 15, 1980)

This paper describes an experimental investigation of the dynamic characteristics of curved wall power fluidics. Two kinds of side wall configurations were examined, namely, a straight side wall (SW) and a curved side wall (AW). The latter wall configuration is based on the attachment stream line, though modified slightly in order to avoid losses. The dynamic experimental studies were performed under various conditions using water of about 20°C as operating fluid. The important results obtained are dynamic responses of the output power relating to the side wall configuration, the main nozzle exit velocity and the offset. The more efficient thruster using AW side wall is designed.

1. Introduction

Side thrusters of a ship or an undersea robot are of effective use in manoeuvring or positioning the craft. The thrusters can be used for direction control, for course holding and for other various operations at low craft speed. In order to develop a more efficient liquid thruster, the curved wall power fluidics are adopted in the present study. The static characteristics of the curved wall elements have been investigated by the authors[1], and the following experimental results have been obtained:

(1) The straight wall elements have the only merit that the flow recovery is better than the curved wall elements. The primary weak point is that such elements have inevitable troubles due to the vortex. The vortex loss decreases pressure recovery and power recovery. The vortex oscillation results in instability for load and noisy output flow. Input sensitivity is also low.

(2) The curved wall elements are more improved in various characteristics except for the flow recovery than the straight wall elements. The low pressure vortex is removed by the curved side wall, so that the pressure recovery, power recovery, stability and output flow condition become better. The input sensitivity is very high.

Referring to the above-mentioned conclusions, the authors develop curved wall thrusters and investigate their dynamic characteristics. Two kinds of side wall studied are (1) the straight side walls (SW) which have various offsets and side wall angles and (2) the curved side walls (AW) with the same offsets and side wall angles. The latter side wall configuration is based on the attachment stream line, though it is modified slightly near the attachment point to reduce the jet impinging loss.

The objects of this investigation are:

---

* Course of Mathematics and Related Fields, College of Integrated General Arts and Sciences.
** Honda Motor Co., Ltd.
*** Chiba Institute of Technology.

1. To clarify the dynamic effects of the curved side wall on performance characteristics such as the output thrust power recovery, the output frequency response and so on.
2. To find hints to the development of more efficient dynamic fluidic devices.

2. Experimental Equipment and Procedure

Fig. 1 shows a schematic diagram of the experimental apparatus. The experimental element was set horizontally at a depth of 20 cm in the water pool and was driven by water of about 20°C supplied from a regenerative pump. The experiments were done at two steps. At the first step, the dynamic behaviours were examined under a constant main nozzle velocity v_s = 5.4 m/s with the main nozzle width b_s = 10 mm (Reynolds number Re = 5.4 x 10^4) and various side wall angles α = 5° - 20° and various offsets D/b_s = 1 - 3. At the second step, the study was directed to clarify the effects of the main nozzle velocity. A smaller and more efficient element was built for this study, referring to the first step. The experiments were done varying the main nozzle velocity v_s in a wide range of 4.0 - 20.0 m/s, with a main nozzle width b_s = 4 mm [Reynolds number Re = (1.6 - 8.0) x 10^4]. The main nozzle flow was regulated by valves and the average flow rate was measured by the use of an orifice and a mercury manometer.

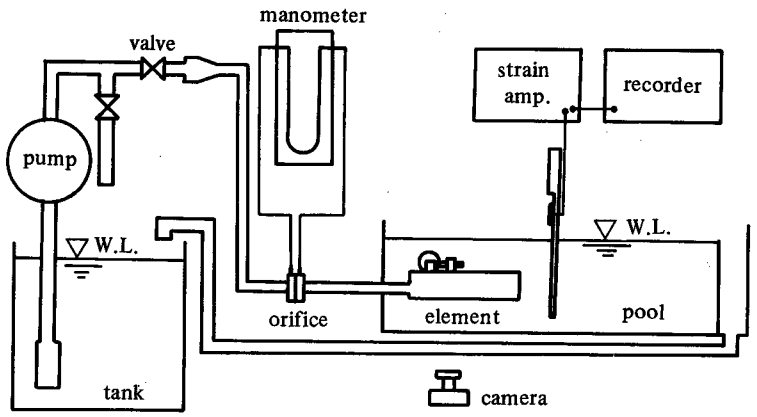

Fig. 1 Schematic diagram of experimental apparatus

The total jet thrust pressure was measured by mean of a strain gauge equiped on the metal plate which was hit by the output jet. The dimension of the metal plate should be properly determined so that the metal plate could catch all amount of the output jet flow.

2.1 Fluidic model

Experimental models of the fluidic element used for investigation are shown in Fig. 2. The model was made of acrylic resin and had the following dimensions: main nozzle width

b_s = 10 mm, control port width b_c = 10 mm, output port width b_o = 20 mm, aspect ratio = 2, offset D = (1 - 3) x b_s (variable) and side wall angle α = 5° - 20° (variable). The shape and position of the splitter are based on the suggestion by M. Ohta et al[2]. Their suggestion was found to be of use. As shown in Table 1, studied combinations of the offset and side wall angle are ten for both SW and AW elements.

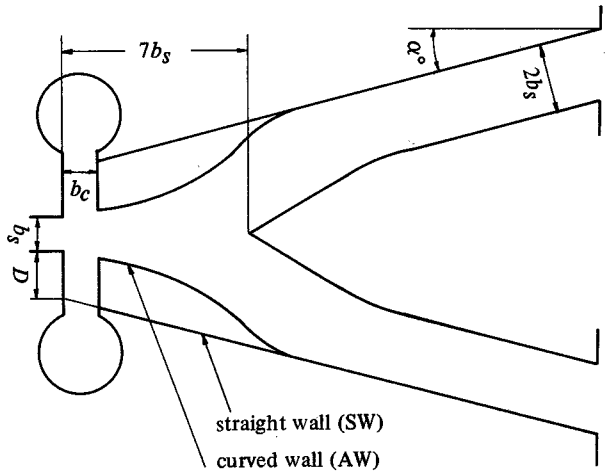

Fig. 2 Experimental model

Table 1. The combinations with offset and side wall angle

D/b_s \ α	5°	10	15	20
1			○	○
2	○	○	○	○
3	○	○	○	○

The figure shows both curved and straight side walls. The curved side wall (AW) is designed on the basis of the attachment stream line observed on the straight side wall (SW) element. The actual curved side wall is offset by 0.1 b_s by considering the spread of the jet at the control port edges and further modified so as to avoid the impingiment loss of the flow using an adequate smooth stream line observed near the attachment point.

The attachment stream line was measured on the SW element by a flow visualization method using the air bubble tracer. The air bubbles were generated by blowing vinyl tubes connected to injection syringes (outer diameter = 0.2 mmϕ) set near the main nozzle exit.

The air bubbles mixed into the stream were illuminated by a wide parallel ray of about 0.5 mm thickness which was projected through the transparent side wall from a narrow slit placed in a slide projector. The trajectories of sparkling bubbles were photographed. This visualization method is very simple though care must be taken of the bubbling not to affect appreciably the liquid specific gravity as well as the pressure distribution.

2.2 Vacuum switching mechanism

Fig. 3 shows the vacuum switching mechanism equipped on fluidic models. The mechanism was made referring to the simplest type in Byrd's paper[3]. The control ports are closed or opened by the flapper which is driven by a pair of solenoids. Each of them is coiled by wire of 0.5 mmϕ diameter by 4000 turns and operated with 100 volts input of rectangular wave. The flapper-solenoids mechanism operated at approximately 35 Hz in water and under no load.

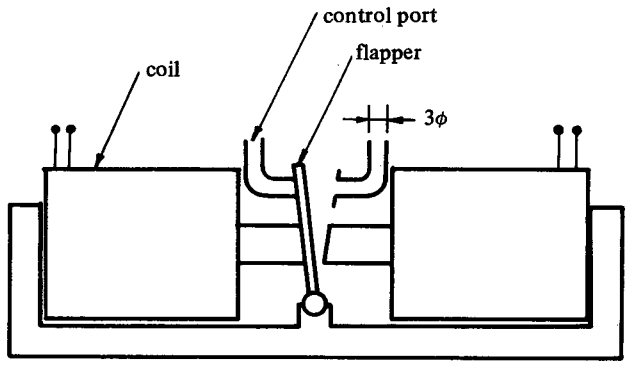

Fig. 3 The vacuum switching mechanism

As Byrd has suggested in his paper, when using a mechanical flapper or armature to open or close the control ports, the problem is to generate enough force to overcome the differential pressure acting on the flapper due to the low pressure in the closed control port. It is to be noted that this differential pressure force affect greatly on the frequency response.

3. Experimental Results

In the study the output power is estimated from the total jet thrust pressure at output ports. Fig. 4 shows the total pressure distributions at the output port exit found for a non-splitter element. The distributions are the static output characteristics for the offset D/b_s = 3 and side wall angle $\alpha = 15°$, under the condition of control flow rate $Q_c/Q_s = 0.2$ (Q_s: main nozzle flow rate). This control flow rate, when used in the dynamic experiment, seems to be not enough to switch the main jet but open the control port only slightly. At any main nozzle exit velocity, the total pressure distribution of the curved side wall is larger than that of the straight side wall, but the profile is not flat. It may be seen from Fig. 4 that the output power can be obtained either by integrating the pressure distribution or by directly measuring the output jet thrust.

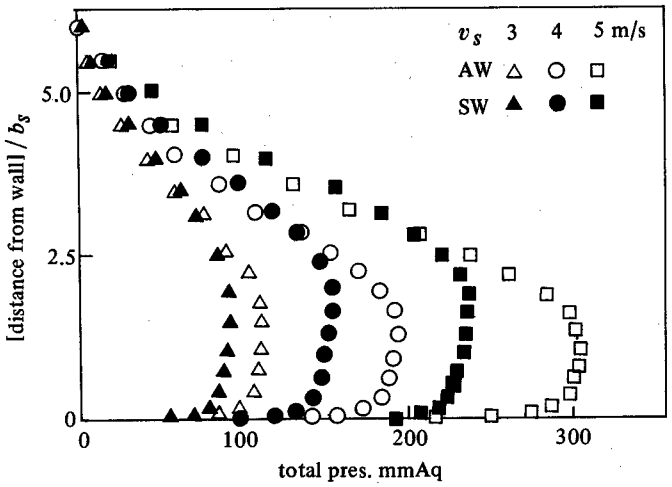

Fig. 4 The total pressure profiles at output port exit

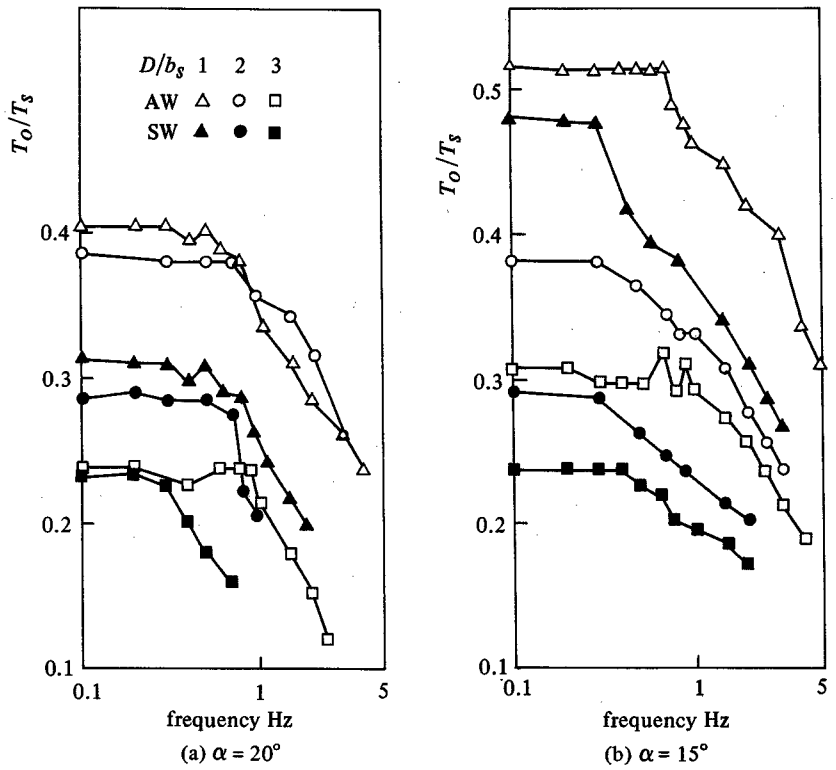

Fig. 5 Frequency response

Figs. 5 (a), (b) show the experimental data (in two cases of $\alpha = 20°$ and $15°$) of the dynamic characteristics of the output jet thrust. The ordinate is the ratio of the output jet

thrust T_O [kg] to the main nozzle exit jet thrust T_S [kg]. Although the data are a little dispersed, the following observations may be obtained: every thrust line is almost constant in the lower frequency zone and begins to decrease at a certain frequency. The break frequencys, at which such a decrease occurs, are slightly higher for the curved side wall element than for the straight side wall element, that is, the former is about 0.9 Hz and the latter is about 0.5 Hz. In the dimensionless output thrust T_O/T_S, the curved side wall element is better than the straight side wall element by about 0.07.

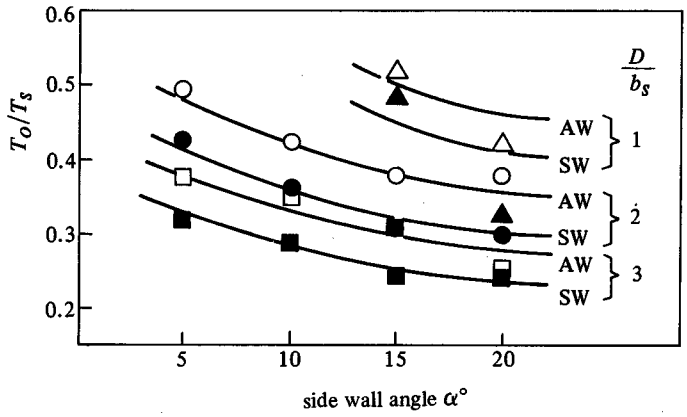

Fig. 6 The relations between output thrust and side wall angle

From twenty original data of SW and AW elements having various offsets or side wall angles, the following two figures are summarized. Fig. 6 shows the relationships between the dimensionless output thrust and the side wall angle. As can be seen from the figure, every curve of AW or SW element is decreasing gradually, at any value of the dimensionless offset, according to increase of the side wall angle α, and becomes lower in the order of the amount of the offset D/b_S. It is also clearly seen from the figure that the thrust of AW element is higher than that of SW element by 0.05 - 0.07 in every case of the offset. The tendency is the same as that in the static output characteristics of the elements. For static performances, the difference of the output characteristics of AW and SW elements depends mainly on the differences of vortex loss and viscosity loss of the side walls. The other internal flow losses are almost in common to AW and SW elements. Therefore, the dimensionless output thrust T_O/T_S of AW and SW elements changes similarly even when the offset and side wall angle are varied, but the output thrust of AW element holds a certain superiority to the output thrust of SW element. Fig. 7 shows the relationship between the break frequency and the side wall angle. Though the data are a little dispersed, the break frequency for AW element seems almost independent of the side wall angles whereas that

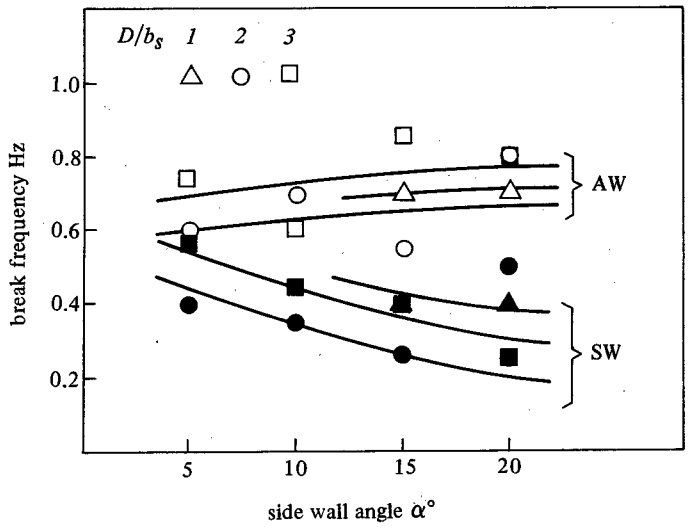

Fig. 7 The relations between break frequency and side wall angle

for SW element becomes lower as the side wall angle increases. The superiority of AW element to SW element is not so apparent in a region of the smaller side wall angle around $\alpha = 5°$, but is notable at larger side wall angles. On the other hand, no clear tendency is seen in regard to the effect of the offset on break frequency. This seems to be the case particularly for AW element and indicates that the concept of the offset can no longer have the same meaning for this element as that for SW element.

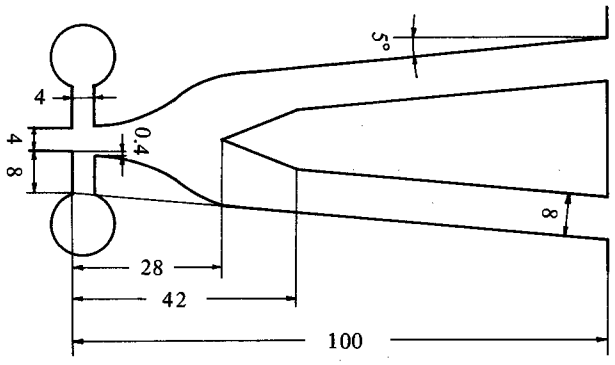

Fig. 8 A new curved side wall element

Referring to the results mentioned above, a new curved side wall element was made, which is shown in Fig. 8. The curved side wall and the shape and the position of the splitter are designed by the same method as mentioned before. The path of the control port is shortened as much as possible in order that the frequency response becomes higher. The principal dimensions are: main nozzle width b_s = 4 mm, aspect ratio = 2.0, control port

width b_C = 4 mm, side wall angle α = 5° and splitter distance = 28 mm. Fig. 9 shows the dynamic characteristics of the output thrust obtained on this element by varing the main nozzle exit velocity v_s. In the lower frequency region, the dimensionless output thrust T_O/T_S does not change even if the main nozzle exit velocity v_s is increased, and the break frequency becomes higher in accordance with increasing the main nozzle exit velocity v_s. The experimental data indicates that the inner flow loss of the element is smaller, that is, the thruster used has efficient at lower frequencies regardless of the main nozzle exit velocity, and further that the dynamic response of the element is improved with increasing the velocity of the operating fluid. Above v_s = 20 m/s, however, the efficiency and response become lower again. This is due to the cavitation occurence and efficiency drop of the vaccum switching mechanism.

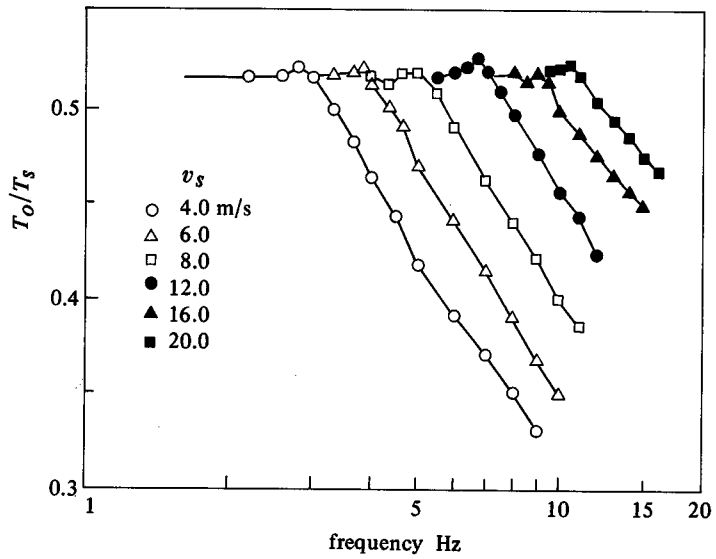

Fig. 9 Frequency response varing the main nozzle exit velocity

4. Conclusions

An experimental investigation was conducted to clarify the dynamic characteristics of the curved side wall necessary for development of a more efficient power fluidic element. Two kinds of side wall used are straight wall (SW) and curved wall (AW). The curved side wall is designed on the basis of the attachment stream line observed on the straight side wall model. The control ports were dynamically closed or opened by the flapper which was driven by a pair of solenoids.

Using water of about 20°C as operating fluid, the experimental study was performed under the conditions of main nozzle exit velocity v_s = 4.0 - 20.0 m/s and various offsets and side wall angles. The twenty kinds of elements were examined, which had various offsets

and side wall angles. The following experimental results are obtained:

(1) The dynamic characteristics were shown as the relationship between the dimensionless output ports jet thrust T_O/T_S (T_S: main nozzle jet thrust) and the operation frequency of the control ports.

(2) The dimensionless jet thrust T_O/T_S below the break frequency of SW and AW elements was summarized as a function of the side wall angle and offset, and the dependence of the break frequency on the same parameters was also given. From these characteristics, AW elements were shown to be improved.

(3) A new efficient fluidic element was built in view of these results and the data was collected of the dynamic characteristics. In accordance with increasing main nozzle exit velocity, the dynamic frequency response was also shown in the relationship between T_O/T_S and input frequency.

References

1) O. Kinoshita and M. Murakami, Bull. of Univ. of Osaka Pref., A 28 1, (1979)
2) M. Ohta, H. Matsuo and M. Kiuchi, Proc. of 3rd National Fluidics Symposium, Kyoto, (1968)
3) J.L. Byrd, Fluidic State of the Art Symposium, (1974)